Time-dependent patterns in the two-layer Rayleigh-Bénard system

Michael M. Degen, Peter W. Colovas, and C. David Andereck
Department of Physics, The Ohio State University, 174 West 18th Avenue, Columbus, Ohio 43210
(Received 26 September 1997; revised manuscript received 7 January 1998)

We report experiments on the two-layer Rayleigh-Bénard system with two different pairs of fluids and with both rectangular and annular geometries. Theoretical studies have shown that in addition to two distinct stationary states, it is possible to have time-dependent patterns at or near convective onset. We have found a traveling wave pattern at the onset to convection using silicone oil over water. Standing and traveling wave states have been found slightly above the onset to convection in a system of silicone oil over Fluorinert™. The basic form of these time-dependent states is consistent with the predictions, while some of the quantitative properties of the states depend on the system geometry. [S1063-651X(98)06306-5]

PACS number(s): 47.20.Bp, 47.27.Te, 47.54.+r, 47.55.Hd

I. INTRODUCTION

The patterns formed in nonequilibrium fluid dynamical systems have long been of interest. (For a recent review of pattern formation, see Cross and Hohenberg [1].) Often, these systems (the Taylor-Couette system with corotating cylinders [2], single-layer Rayleigh-Bénard convection [1], flow past a cylinder [3], the Taylor-Dean system [4], the Weissenberg effect [5], etc.) bifurcate initially to one or more stationary states and then eventually to a time-dependent state as the appropriate control parameter is increased. In these cases, time-dependent patterns typically appear at values of the control parameter significantly above the value for the onset to the first stationary pattern. Unfortunately, this difference between the control parameter values for the onset to time dependence and the value for the onset to a stationary pattern precludes an analysis of the linearized equations of motion to describe the time-dependent states. It is therefore desirable to investigate an experimental system that exhibits time dependence at or near the onset to a pattern. There are cases where time dependence occurs at or just above pattern onset, as, for example, in the Taylor-Dean system [4], binary fluid convection [6], the Taylor-Couette system with counter-rotating cylinders [2], and Rayleigh-Bénard convection with small Prandtl number fluids [1]. Such a time-dependent state is predicted for the two-layer Rayleigh-Bénard system [7], a system that is accessible experimentally, and for which theoretical analysis is feasible.

One of the most extensively studied examples of pattern forming fluid dynamical systems is the single-layer Rayleigh-Bénard system [8]. The classic Rayleigh-Bénard system consists of a horizontal layer of fluid bounded above and below by planar surfaces. The bottom surface is maintained at a temperature T_0 and the top surface is maintained at a (typically) lower temperature $T_0-\Delta T$. A theoretical analysis by Rayleigh [9] found a parameter

$$\mathrm{Ra}=\frac{g\alpha\Delta T d^3}{\nu\kappa} \tag{1}$$

(later given the name Rayleigh number) which serves as the nondimensional control parameter for this system with g as the acceleration due to gravity, α the coefficient of thermal expansion, d the height of the layer, ν the dynamic viscosity, and κ the thermal diffusivity. A second parameter, the Prandtl number ($\mathrm{Pr}=\nu/\kappa$), plays a role in determining the states above onset. In a typical experiment (with rigid upper and lower surfaces), the onset pattern takes the form of stationary convection rolls (exceptions occur with low Pr fluids or non-Boussinesq flows [1]). Time dependence does not appear in typical experiments until at least $\mathrm{Ra}>2\mathrm{Ra}_c$. High Pr fluids require $\mathrm{Ra}>100\mathrm{Ra}_c$ or more [10] before the onset to time-dependent patterns.

In contrast to single-layer Rayleigh-Bénard convection, which is described by Ra and Pr, the simple act of adding a second layer of immiscible fluid to the system opens up a vast parameter space that is yet to be thoroughly explored. The flow in a two-layer system not only depends on a Ra and Pr for each layer, but also depends on the heights of the fluid layers and all of the fluid parameters (thermal conductivity, thermal expansion, viscosity, etc.). Additionally, new driving mechanisms associated with the interface (surface tension and/or deformation) could play a role in the dynamics. These new factors combine to produce new flow states which cannot be found in the single-layer system. Many of these new states are described in the text by Renardy and Joseph [11]. One of the more interesting predictions is the possibility of finding time-dependent states at the onset to convection. In such a case, weakly nonlinear equations could be used to describe the patterns, an exciting prospect which makes the theoretical problem of studying time-dependent patterns considerably more tractable. In contrast, time-dependent states only appear well above onset in the one-layer Rayleigh-Bénard system (high Pr), where the fully nonlinear equations apply.

Much of the interest in multiple-layer Rayleigh-Bénard convection has been inspired by two practical problems, namely, mantle convection and encapsulated crystal growth. The Earth's mantle is modeled in one of three ways: single layer, two layer, and two layer with flushing events. The first model is virtually identical to the single-layer Rayleigh-Bénard system. The second model is similar to the system studied here, while the third is a hybrid of the first two models. Much theoretical work has been done on the two-layer model of mantle convection [12–16], however, experimental

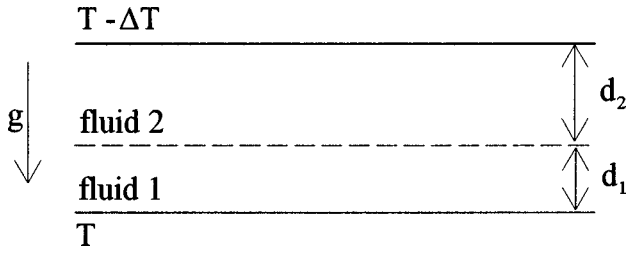

FIG. 1. Schematic diagram of the two-layer Rayleigh-Bénard system. g is the acceleration due to gravity, d_1 and d_2 are the lower and upper layer depths, the solid lines indicate the presence of thermally conducting solid top and bottom boundaries at the temperatures indicated, and the dashed line is the interface between the two fluids.

data are quite limited. The second system, encapsulated crystal growth [17], concerns the solidification of a crystal which is bounded above and below by fluids. It is necessary to understand the flows associated with such a system in order to ensure the desired crystal characteristics. Experimental studies with the two-layer Rayleigh-Bénard system will provide useful information for dealing with both of these practical problems.

The two-layer Rayleigh-Bénard system is shown schematically in Fig. 1. By convention, the bottom layer is labeled 1 and the top is 2. All quantities specific to each layer will have the appropriate subscript, i.e., the bottom layer viscosity will be ν_1, the top layer viscosity will be ν_2, etc. Two new quantities come into the problem to describe the relative height of the layers. The ''depth fractions'' are defined as

$$l_1=\frac{d_1}{d} \text{ and } l_2=\frac{d_2}{d}=1-l_1 \tag{2}$$

representing the height of each layer relative to the overall height [18]. An alternative form is the ''depth ratio,'' given as

$$a=\frac{d_2}{d_1}=\frac{l_2}{l_1}, \tag{3}$$

which is the ratio of the height of the top layer to that of the bottom [19]. In addition to the heights of the layers, Renardy [20] has shown that the fluid parameters enter into the equations of motion in the ratios

$$m=\frac{\mu_1}{\mu_2}, \quad r=\frac{\rho_1}{\rho_2}, \quad \gamma=\frac{\kappa_1}{\kappa_2}, \quad \zeta=\frac{k_1}{k_2} \text{ and } \beta=\frac{\alpha_1}{\alpha_2}, \tag{4}$$

where μ is the kinematic viscosity, ρ the density, and k the thermal conductivity.

Analysis of the linear equations by Colinet and Legros [19] for a specific value of the fluid parameter ratios yields a bifurcation diagram which shows the possibility of three states depending on a, the depth ratio [Eq. (3)] of the two fluids (or alternatively l_1 the depth fraction). They found that above ΔT_c (or Ra_c), each layer forms its own set of convection rolls, similar to those in the single-layer Rayleigh-Bénard system. The different flow states at onset in the two-layer Rayleigh-Bénard system concern the alignment or coupling of the two sets of rolls. More recently, Renardy [20] analyzed another set of fluid parameter ratios and produced the bifurcation diagram shown in Fig. 2. The fluid parameters were chosen to illustrate the basic possible convective onset states.

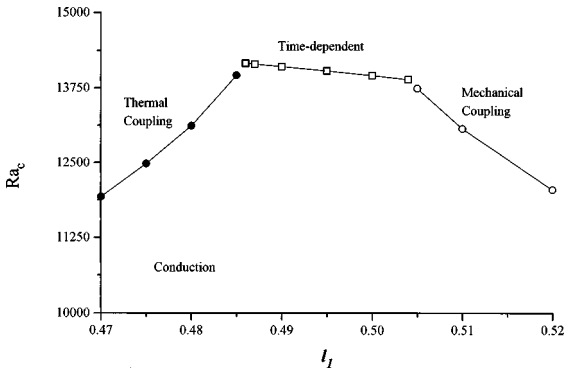

FIG. 2. Critical bifurcation diagram from Renardy [20] for a particular set of fluid parameters, chosen to illustrate the basic possible convective onset states. The possible onset states are thermal coupling (●), mechanical coupling (○), and time dependent (Hopf modes) (□). Renardy defines $\mathrm{Ra}=g\alpha_1\Delta T d^3/\kappa_1\nu_1$.

Two of the simplest possible flow states are stationary and are shown in Fig. 3. The first is called ''mechanical coupling'' (MC) (or alternatively viscous coupling). MC is the state where hot upflow in one layer is above (or below) cold downflow in the other layer. The fluid flows in the same direction above and below the interface, i.e., the rolls rotate

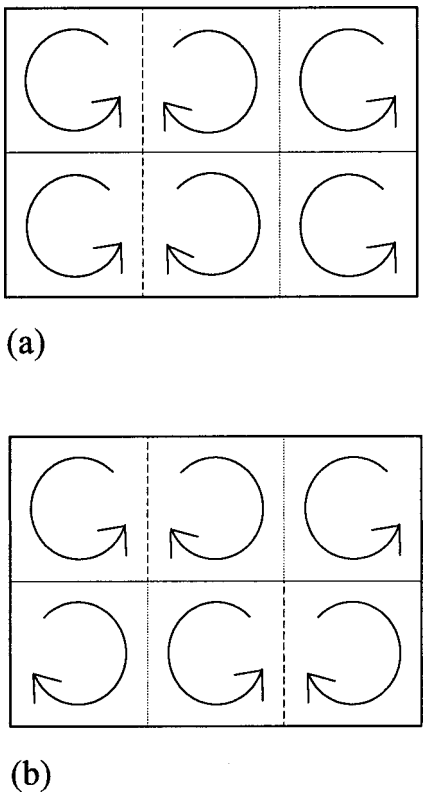

FIG. 3. Cartoon of the stationary states found in the two-layer Rayleigh-Bénard system. (a) Thermal coupling, (b) mechanical coupling.

in a gearlike fashion. The second stationary state is called ''thermal coupling'' (TC). TC is characterized by the hot upflow in one layer being above (or below) the hot upflow in the other layer. Likewise, the cold downflows are also aligned, forcing the rolls to turn in opposite directions above and below the interface, thereby setting up a region of high shear. The third basic state found in the two-layer system is time dependent, as shown by Gershuni and Zhukovitskii [7]. As further described by Colinet and Legros [19], it takes one of two forms depending on the exact nature of the experimental configuration. In confined systems, the time-dependent state is an oscillation between MC and TC, while in extended systems it manifests itself as a traveling wave state that is neither exactly TC nor MC.

It turns out that the generic characteristics of Fig. 2 are robust: TC is present at low values of l_1, MC is at high values of l_1, and between the MC and TC is a region of time dependence. The exact details of the size of the time-dependent regime and its location are dependent on the particular values of the fluid parameters [7,19,21,20,22]. For some sets of fluids, the time-dependent region is so small as to be practically inaccessible to experiments or possibly even nonexistent at the onset to convection.

Further analysis of the two-layer problem looking at the weakly nonlinear and fully nonlinear equations has been carried out by many researchers [19,23,24,11,25,26,20,18]. They have shown that, in addition to the states described above (TC and MC), a system with an extended geometry (both horizontal dimensions are large compared to the height) can have a variety of three-dimensional patterns. An extensive listing of these can be found in the text by Renardy and Joseph [11]. Other authors have investigated the effects of surface tension and/or deformable interfaces [27,16,13–15,12]. The interesting idealized case of a 1:2 ratio in the pattern wavelengths has been studied by Proctor and Jones [28].

Previous experiments

Experimental work on the two-layer Rayleigh-Bénard system has been carried out by a number of researchers. One of the first investigations was by Zeren and Reynolds [27]. They report confirmation of the theoretical prediction for Ra_c when heating from below, but heating from above did not show any of the predicted instabilities. This work predates the theoretical prediction of a time-dependent onset. Later work by Rasenat, Busse, and Rehberg [21] appears to have been in a parameter range near, but not in, the time-dependent region. They investigated the flows at values of l_1 just below and just above the predicted oscillatory region. Experiments by Prakash and Koster [29] have concentrated on the mechanisms associated with the two distinct stationary coupling modes (TC and MC) and how they vary with fluid properties. Prakash and Koster do not report a time-dependent state. Cardin and co-workers [30–32] have reported a time-dependent state. However, their state does not involve coupling oscillations and has characteristics far from those predicted by linear theory. For example, the observed period is 20 h compared to predicted periods on the order of 1 h. Secondly, the reported onset to the time-dependent state is at $\mathrm{Ra}=9.7\mathrm{Ra}_c$, well above the predicted onset. An observation of the predicted state has been reported by Andereck, Colovas, and Degen [33,34] and Colovas [35]. Recently, Busse and Sommerman [36] have also reported observations of a time-dependent state in an annular system using thermistors to probe the flow.

II. APPARATUS

Two experimental systems have been constructed with distinct geometries. The first is rectangular in form and the second is annular. The dimensions of both systems were chosen to force the rolls in each fluid layer to align parallel to the smaller horizontal dimension of the convection cell, i.e., the width of the rectangular system is small compared to the length and the radial gap size of the annulus is small compared to the circumference. In these geometries the flow patterns are forced to be approximately two dimensional. Both systems use optical methods to probe the flow from the side. The typical single-layer Rayleigh-Bénard experiment uses top-down visualization. However, a top-down scheme would be difficult to implement and interpret with two layers and hence the choice of a horizontal method.

A. The rectangular system

The top and bottom surfaces of the rectangular system consist of aluminum blocks. The top block has width 48 mm, length 137 mm, and height 48 mm, while the bottom has the same width and length, and a height of 55 mm. The blocks are thick to assure uniformity of temperature across the surfaces in contact with the fluids. The top and bottom blocks are cooled and heated, respectively, by water that is conditioned by commercially available recirculating temperature controlled baths. The water flows along the long axis of each block, through a $\frac{1}{2}$-in.-diam hole. The thickness of the blocks assures that any variation of the temperature across their short dimension is minimized. Both of the baths have temperature uniformity of $\pm 0.1\,^{\circ}\mathrm{C}$. For both plates, the temperature regulation circuits are completed by thermal low-pass filters and active heaters to further reduce the fluctuations in the downstream temperature. The thermal low-pass filters are essentially large insulated boxes where water just exiting from the chiller mixes with water processed earlier to smooth out the short-time transients produced by the bath. The active heaters are 100 Ω of Teflon-coated nichrome wire packed into acrylic tubes and inserted into the fluid path. They are driven by a Quantum Design model 1802 R/G bridge which implements a proportional integro-differential (PID) control scheme. Using these devices, the stability of the temperature difference ΔT is better than $\pm 0.005\,^{\circ}\mathrm{C}$. The temperature variation across the surface of a block is less than $\pm 0.005\,^{\circ}\mathrm{C}$. The temperature difference between the plates is measured by thermistors embedded in the center of each block.

The sidewalls of the system have taken various forms. The first setup used sidewalls which were constructed of $\frac{3}{8}$-in. soda-lime glass. The interior horizontal dimensions of the cell are nominally 78 mm×21 mm, with the total height of the cell $d=12$ mm. A second setup uses Plexiglas cells of the same nominal dimensions. These cells have the added feature of a groove machined into the inside of the cell to pin the interface between the fluids at the sidewalls to the pre-

scribed depth ratio, alleviating the problem of meniscus effects discussed below.

B. The annular system

Like the rectangular system, the top and bottom surfaces are made from aluminum, due to its high thermal conductivity. The top plate is annular with outer diameter 161 mm, inner diameter 59.1 mm, and height 44 mm. Water is circulated through the top ring to maintain its temperature. The temperature of the water is maintained with a commercially available temperature bath and a thermal low-pass filter as with the rectangular system. No active heaters were used with the annular system. A series of thermistors is embedded into the plate to allow monitoring of the temperature.

The outer and inner radii of the bottom plate are the same as the top plate. However, the height of the bottom plate is 25.4 mm. The temperature of the bottom plate is maintained via a film heater. The current supplied to the film heater is regulated by a computer using a PID scheme and a linearly programmable power supply. This method of temperature control gives a long-time stability of ΔT that is better than $\pm 0.007\,^{\circ}\mathrm{C}$, comparable to that in the rectangular system.

The working fluids are contained between two Plexiglas rings. The outer ring has outer diameter 139.5 mm and inner diameter 126.6 mm. The inner ring has outer diameter 88.8 mm and inner diameter 76.1 mm. Both have a height $d = 12.2$ mm. The gap is 18.9 mm wide and the aspect ratio $\Gamma = 2\pi r_m/d = 27.7$, where $r_m = 53.9$ mm is the mean radius.

C. Visualization

Visualization of the flow pattern in both geometries is achieved using the shadowgraph method. Some experiments with the rectangular system have also used the schlieren method. For a discussion of both methods see the text by Goldstein [37], and for shadowgraphs see Jenkins [38].

Shadowgraphs are sensitive to variations of the index of refraction of the fluid due to variations in the temperature. Regions of hot fluid (i.e., upward flows) defocus the light and appear dark in the resulting image. Cold fluids (i.e., downward flows) act the opposite and focus the light, thus appearing bright in the image.

As noted previously, the typical implementation of the shadowgraph method for single-layer Rayleigh-Bénard convection is to view from above. Since shadowgraphs are integral along the direction of propagation, it would be difficult to separate the behavior of the two layers using this approach. To alleviate this, it was decided to view the flow from the side. In an annular geometry, this requires viewing in a radial direction.

The portion of the annular apparatus used to observe the flow follows from [39] and is shown in cross section in Fig. 4. A light-emitting diode (LED) is positioned at the focal point of a lens, which produces collimated light. This collimated light travels down the axis of the system where it reflects off of a 45° conical mirror, giving radially outward propagating light. Next, the light traverses the Plexiglas rings and the convecting fluids. Then the light is reflected back radially inward by a cylindrical mirror. The light makes a second pass through the fluid before striking the conical mirror again to exit the system along the axis. A portion of the

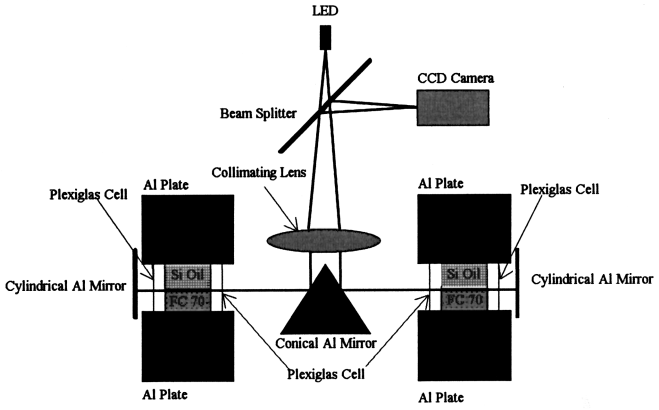

FIG. 4. Schematic diagram of the annular apparatus.

light is directed into a Pulnix TMC-7CN charge-coupled device (CCD) camera with a beam splitter. The CCD camera is connected to a 386 computer via an 8-bit image acquisition board (Imaging Technology's FG-100-AT) that captures images and time series data.

Using this method to probe the system produces images such as that in Fig. 5. Moving radially outward from the center, the first ring of alternating bright and dark lines represents the roll structure in the top fluid layer. The next fuzzy ring is the interface, and finally the outer ring of alternating bright and dark lines is the roll structure in the bottom layer.

Implementation of the shadowgraph method in the rectangular system, shown in Fig. 6, is similar to that used with the annular system, albeit much simpler due to the need for only planar mirrors. A second visualization method was originally used with the rectangular system, namely, the schlieren method. The schlieren method begins with collimated light passing through the system. Next, the light is refocused by a second lens. A knife edge is positioned at the focal point and blocks a portion of the light. The light is captured by a CCD camera as it reexpands beyond the focal point.

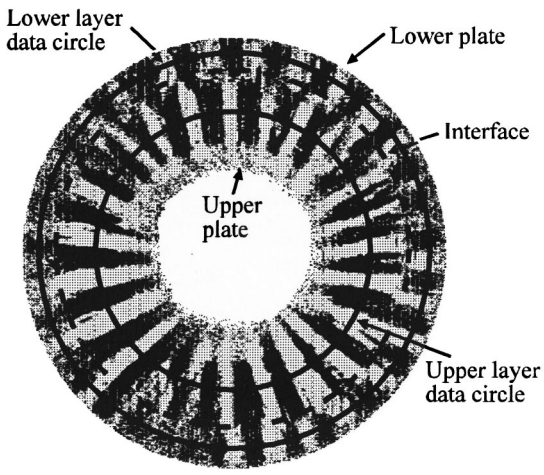

FIG. 5. Sample image from the annular two-layer Rayleigh-Bénard system in the time-dependent regime. The image has been divided by a background image at $\Delta T = 0$ to remove any optical defects. Note, this state has TC at the bottom right and MC at the top. The solid lines show the circles of data captured for time series files. The dashed line is the location of the interface between the two fluid layers.

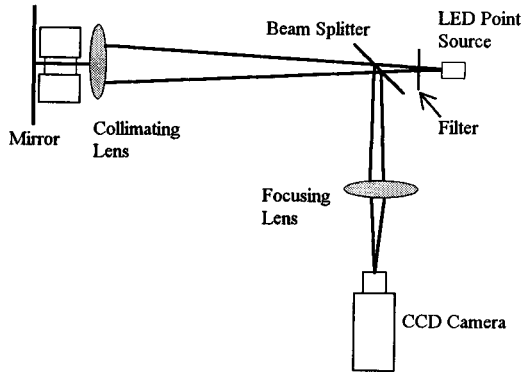

FIG. 6. Schematic diagram of the visualization system used with the rectangular system.

Like shadowgraphs, the schlieren technique is also sensitive to variations in the index of refraction. As the light passes through the fluid, horizontal variations of the index bend the light. Any light that is bent toward the knife edge is blocked, while light bent away from the knife edge passes, yielding an image such as Fig. 7. Here bright regions represent rolls with hot fluid on, say, the left and cold fluid on the right. The dark regions would correspond to the opposite, namely, hot on the right and cold on the left.

III. FLUID SELECTION

The most important elements of the experiment are the fluids. Great care must be exercised in the selection process. Several factors are taken into consideration, including immiscibility, optical properties, meniscus effects, and the onset Rayleigh number [see Eq. (1)]. A final selection criterion is from recent work by Renardy [20]. Renardy defines a parameter $\gamma\beta r$, based on the fluid properties in Eq. (4), that must be far from 1 to maximize the parameter window for finding a time-dependent onset. $\gamma\beta r$ is a measure of the self-adjointness of the equations describing the system. A fluid combination with $\gamma\beta r=1$ is characterized by self-adjoint equations and the eigenvalues will be real. The further $\gamma\beta r$ is from 1, the less self-adjoint the equations are, and the more likely will be a time-dependent onset [20].

The immiscibility criterion is necessitated by the use of two layers of fluid with a distinct interface. While no two fluids are ever 100% immiscible, some combinations can be close.

The requirements on the optical properties follow from the use of the visualization methods. First, the fluids must be clear to allow the light to propagate through them. Second, the variation of n with temperature must be large enough to produce detectable image brightness variations.

As shown in [40,21], meniscus effects can have a large impact on convective flows. Ideally, the contact line between the two fluids would be perpendicular to the side wall and straight. If the contact line is not straight or the meniscus too large, the variations in the heights of the two layers can change the flow states. These variations can be minimized by the fluid selection as well as by the proper choice of the sidewall material.

The last criterion rests on the search for the oscillatory onset and that the fluids follow the Boussinesq approximation near onset. The latter requirement dictates that the critical temperature difference ΔT_c have a reasonable value. As shown in Colinet and Legros [19], one criterion for the oscillatory onset is that the critical Rayleigh numbers Ra_c in each layer be approximately equal. Since the temperature of the fluids at onset is nearly the same as in the conduction state, the so-called ''conduction assumption'' can be used to calculate the interface temperature between the two fluids. This method assumes that each fluid is merely conducting heat from the bottom plate to the top and the interface temperature is determined by Newton's law of thermal conduction. Use of this assumption gives an interface temperature of

$$T_{\mathrm{int}}=\frac{d_2k_1(T_0-\Delta T)+d_1k_2T_0}{d_2k_1+d_1k_2}. \tag{5}$$

This definition for the interface temperature can be used to slightly modify Eq. (1) to define Rayleigh numbers for each layer as

$$\mathrm{Ra}_1=\frac{g\alpha_1(T_0-T_{\mathrm{int}})d_1^3}{\kappa_1\nu_1} \quad \text{and}$$

$$\mathrm{Ra}_2=\frac{g\alpha_2[T_{\mathrm{int}}-(T_0-\Delta T)]d_2^3}{\kappa_2\nu_2}. \tag{6}$$

Setting $\mathrm{Ra}_1=\mathrm{Ra}_2$ and folding in Eq. (5) allows a calculation of the relative depths of the two layers at which the onset coincides.

Since the experiments began before Renardy's work describing $\gamma\beta r$ [20], the initial search only concentrated on the first criteria and did not include an analysis of $\gamma\beta r$. A long search finally led to the combination of Rhône Poulenc's Rhodorsil™ 47v10 silicone oil over 3M Corporation's Fluorinert™ FC70. FC70 is a perfluorinated hydrocarbon that is essentially chemically inert. Both of these fluids are clear and their physical properties appear in Table I. They produce a reasonably small meniscus and a straight contact line with

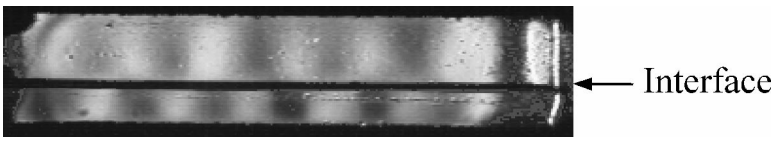

FIG. 7. Sample schlieren image from the rectangular FC70-47v10 system at $\Delta T=1.6\,^{\circ}\mathrm{C}$, $l_1=0.38$. The labeled arrow indicates the level of the interface between the fluid layers. The light regions in each layer indicate rolls turning in one direction (say clockwise) and the dark regions indicate rolls turning in the opposite direction. The alignment of dark regions over light and vice versa shows mechanical coupling.

TABLE I. Physical properties of the 47v10 and FC70 fluids. Data taken from specification sheets provided by the manufacturers.

	cgs units	47v10	FC70
Density ρ	$g\ cm^{-3}$	0.927	1.94
Kinematic viscosity ν	$cm^2\ s^{-1}$	0.10	0.14
Thermal diffusivity κ	$cm^2\ s^{-1}$	8.601×10^{-4}	3.446×10^{-4}
Thermal expansion α	K^{-1}	1.08×10^{-3}	1.0×10^{-3}
Thermal conductivity k	$g\ cm\ s^{-3}\ K^{-1}$	1.3×10^{4}	0.70×10^{4}
Specific heat C_p	$cm^2\ s^{-2}\ K^{-1}$	1.63×10^{7}	1.047×10^{7}

the Plexiglas or glass sidewalls. Calculation of the onset Rayleigh number gives $\Delta T_c \sim 0.76\ °C$ and $l_1 = 0.43$, both reasonable values.

After the publication of Renardy's paper [20], a calculation showed that the FC70–47v10 system has $\gamma\beta r = 0.776$, which, while not exactly one, makes finding a Hopf bifurcation at onset very difficult. It turns out that many of the fluids with the kinds of desirable mechanical properties mentioned above are similar enough to each other to have $\gamma\beta r \approx 1$. A second search using all of the criteria led to the combination of water beneath 2 cS silicone oil, Rhône Poulenc's Rhodorsil 47v2, for which $\gamma\beta r = 0.375$. Additional properties of the water-47v2 system are listed in Table II.

Unfortunately, the water-47v2 combination presents other experimental difficulties. Primarily, water has a high surface tension, while the 47v2, on the other hand, wets most surfaces. This combination of properties results in the water beading up in the bottom of the cell, while the oil reaches down the sidewalls all the way to the bottom plate. Our solution to this dilemma is to force the water into a flat interface through the addition of a groove along the inside of the sidewalls at the desired depth of the water. This procedure is an effective way of pinning the meniscus at the walls, and works for groove widths as small as 1.59 mm. The depth of the groove is approximately 1.27 mm. One drawback to this approach is that it introduces some uncertainty into the exact position of the interface. The meniscus in the FC70-47v10 system, using an ungrooved glass or Plexiglas cell, is ~ 1 mm thick. The groove increases that width by some 50%, which is acceptable since having a flat interface is of paramount importance in providing uniform spatial conditions for the pattern formation process, and to prevent pinning of the time-dependent states. Unfortunately, using water presents another difficulty in that its variation of index of refraction with temperature is small, making simultaneous shadowgraph visualization of both layers difficult.

IV. EXPERIMENTAL PROCEDURE

A. The rectangular system

Once the fluids are selected, the experimental variables are reduced to the depths of the layers, l_1 and l_2, and the temperature difference ΔT between the top and bottom plates. We proceed by selecting fluid depths, and slowly ramping the temperature difference from $\Delta T = 0$. In the FC70-47v10 system, the depth of the lower fluid is measured precisely by an optical telescope, accurate to ± 0.02 mm. The full system is left to equilibrate for a period of 12 h before the temperature ramping begins.

Following the equilibration period, a data series is initiated. A data series begins by ramping ΔT by 0.1 °C and waiting ~ 6 h for the system to reach a steady state. After the wait, a full image is stored and a data file is begun. A data file consists of a horizontal line of high contrast in each layer recorded at 30-sec time intervals (15-sec intervals for the water-47v2 combination). Each data file typically has 512 or 1024 lines. Two data files can be captured per day, leading to a total daily temperature change of 0.2 °C. Near the onset to convection, the increment in ΔT is reduced to 0.025 °C with the same wait periods.

The resulting data can be displayed as an intensity plot, as in Fig. 8. Each line represents a single time step, with time running up the vertical axis, and space on the horizontal axis. The variation of the line represents the intensity of the shadowgraph at that point.

The space-time data are used to compute the power spectra in space and time, which yield the wavelength and frequency of the pattern at each depth fraction and ΔT. The power spectrum is an average taken over the entirety of the run, i.e., if the wave number is being computed, it is a time-averaged wave number, while if the period is being computed, it is spatially averaged over the long dimension of the cell. In computing the periods and wave numbers of the time-dependent states, a time average at each spatial point is

TABLE II. Physical properties of the fluids in the water-47v2 silicone oil system.

	cgs units	47v2	Water
Density ρ (at 25 °C)	$g\ cm^{-3}$	0.867	0.998
Kinematic viscosity ν	$cm^2\ s^{-1}$	0.02	0.01
Thermal diffusivity κ	$cm^2\ s^{-1}$	7.78×10^{-4}	0.001
Thermal expansion γ	K^{-1}	1.17×10^{-3}	2.067×10^{-4}
Thermal conductivity k	$g\ cm\ s^{-3}\ K^{-1}$	1.1×10^{4}	5.98×10^{4}
Specific heat C_p	$cm^2\ s^{-2}\ K^{-1}$	1.63×10^{7}	4.1818×10^{7}

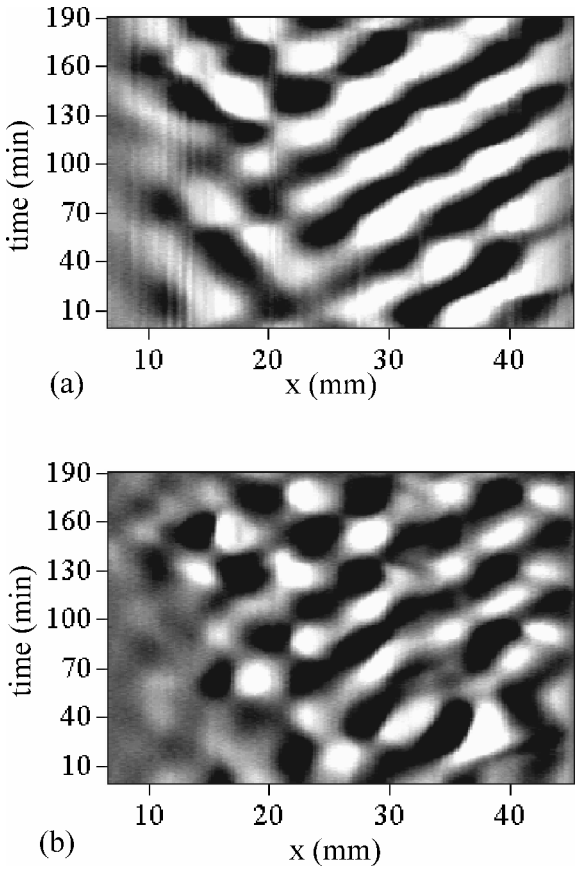

FIG. 8. Space-time plot of the (a) top and (b) bottom layer from the rectangular system, same state as shown in Fig. 7. Time advances up the vertical axis, and a time-averaged background has been subtracted.

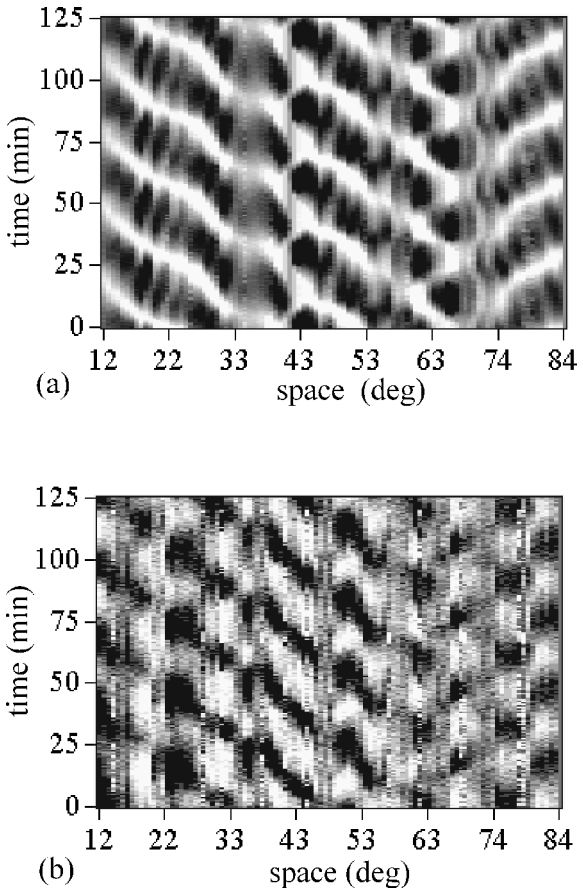

FIG. 9. Background-subtracted space-time diagram from the annular system showing the smooth roll motion just above onset at $\Delta T = 1.103\,^{\circ}\mathrm{C}$, $l_1 = 0.375$. (a) is upper layer. (b) is lower layer. Vertical axis is time (min). Horizontal axis is θ (°) around cell. Notice a source is located at $\approx 65°$.

subtracted from the data to remove nonuniformities due to the optics and lighting. When possible, spectra are also computed without background subtraction for comparison.

B. The annular system

The procedure used with the annular system is nearly identical to that used with the rectangular system. The only difference is in the space-time data. Instead of capturing a straight line through the image, circles are captured. (A schematic of this is shown in Fig. 5.) The circles are straightened and plotted as space-time diagrams identical to those from the rectangular system. Some representative space-time diagrams are seen in Figs. 9–11.

V. EXPERIMENTAL RESULTS

A. The annular system

The primary results of this work are summarized in flow regime diagrams showing ΔT vs l_1 for transitions to the various patterns. (The data are presented in terms of ΔT, not Ra, due to the many alternative definitions of Ra which exist in the literature describing the two-layer Rayleigh-Bénard system.) The first of these is Fig. 12, obtained for the case of 47v10 silicone oil over Fluorinert FC70. Time-dependent convection is found in the range $0.357 \leqslant l_1 \leqslant 0.382$ at a ΔT roughly 0.1 °C above the onset to stationary convection. Unfortunately, the desired result of time dependence at the onset to convection has not been found with this set of fluids. However, a theoretical analysis by Renardy [20] for this specific set of fluids has shown that this is the expected result.

The stationary convection for $l_1 < 0.357$ shows strong evidence of thermal coupling while states with $l_1 > 0.382$ show stationary mechanical coupling. This orientation, with TC at low l_1, MC at high l_1, and time dependence in between, confirms the general prediction of Colinet and Legros [19]. It should be noted that these states have been explored to at least $\Delta T = 2\,^{\circ}\mathrm{C}$ (twice the onset to convection) and sometimes to $\Delta T = 3\,^{\circ}\mathrm{C}$. The time-independent states are stationary throughout the range of ΔT.

The period (τ) of the time-dependent state, found from analysis of the power spectra, is shown in Fig. 13(a). The data show an increase from $\tau \sim 50$ min at low ΔT to $\tau \sim 80$ min at higher ΔT.

The wavelength (λ) of the pattern, found from analysis of the power spectra, is shown in Fig. 13(b) as a function of ΔT. It is evident that the wavelength is roughly constant over the range of ΔT with a value of $\lambda = 15.6° = 14.7$ mm. The wavelength can be expressed in terms of Renardy's dimensionless wave number $\alpha = 2\pi d/\lambda = 5.2$.

Inspection of Figs. 9 and 10 shows that both have roll sources present. In Fig. 9, the source is at 65° (relative to an arbitrary 0 point) while in Fig. 10 the source is at 43° (relative to the same 0 point). These figures were captured se-

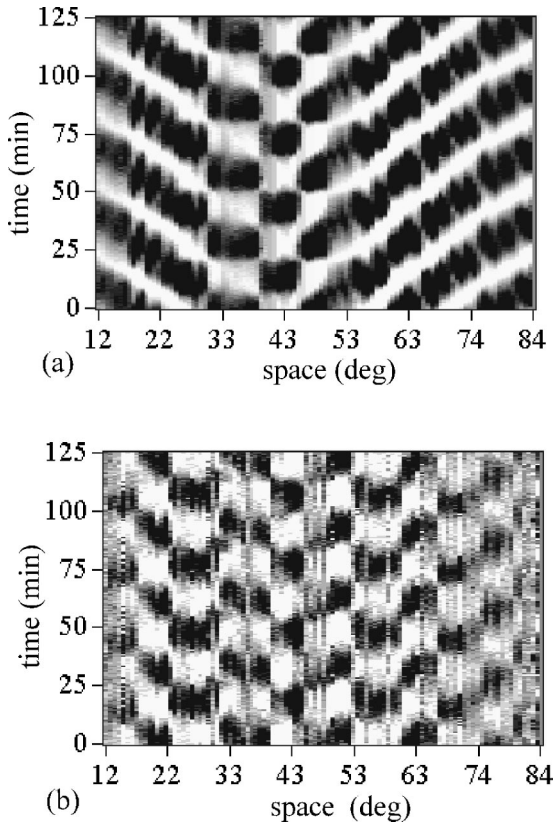

FIG. 10. Background-subtracted space-time diagram from the annular system showing smooth roll motion somewhat farther above onset than for Fig. 9 at $\Delta T = 1.189\,^{\circ}\mathrm{C}$, $l_1 = 0.375$. (a) is upper layer. (b) is lower layer. A source is located at $\approx 45°$.

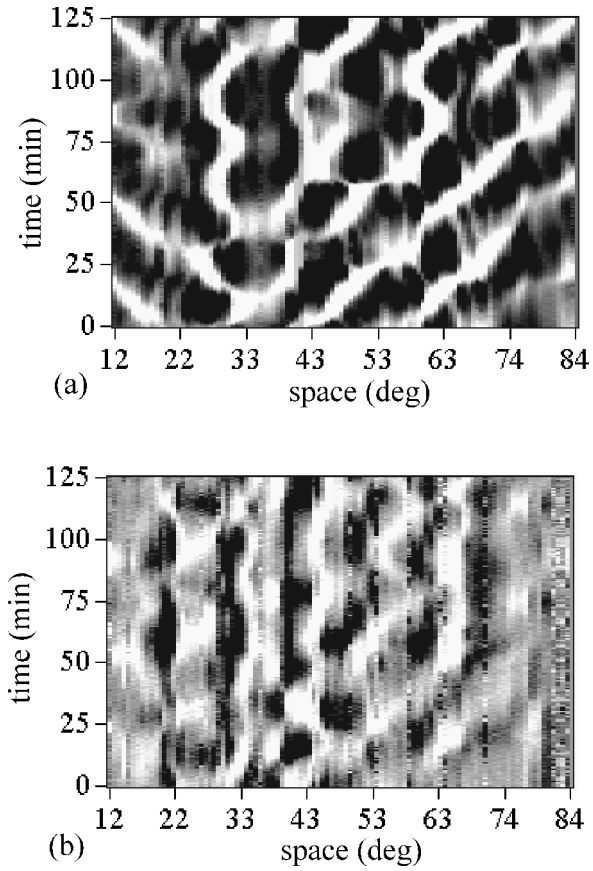

FIG. 11. Background-subtracted space-time diagram from the annular system showing roll motion at $\Delta T = 1.567\,^{\circ}\mathrm{C}$, $l_1 = 0.375$. (a) is upper layer. (b) is lower layer. The motion of the rolls is highly irregular and can be seen to change direction.

quentially with only a 0.1 °C increase in ΔT between them. The location of the source is chosen by the flow and is not pinned by any features found in the system. Furthermore, corresponding sinks can also be found in the system. It should be noted that all of the observed time-dependent states contained two or three source-sink pairs. States with no sources or sinks were never observed.

Further analysis of the time-dependent state focuses on the positions of the roll boundaries and their motion. For ΔT near onset, the roll motion is relatively smooth and linear (Figs. 9 and 10). At higher ΔT, the roll motion becomes irregular (Fig. 11). In other words, the velocity is relatively constant over long periods for ΔT near onset while the velocity changes with time at higher ΔT. To analyze this in more detail, a program was written to find the downflow boundary, which appears in the space-time diagrams as a high value. Figure 14 shows one representative roll boundary from Fig. 10 and one roll boundary from Fig. 11. It is clear from Fig. 14 that the roll motion at high ΔT is much more complicated than for ΔT near onset. This particular roll actually changes its direction of motion during the data set. To further emphasize this difference, the velocity of the rolls in Fig. 14 is shown in Fig. 15. The motion from ΔT near onset has a relatively constant velocity while the roll at higher ΔT exhibits a slow velocity $v_s \approx 0.12$ mm/min and a fast velocity $v_f \approx 0.45$ mm/min. This fast-slow or stick-slip motion is qualitatively similar to the ''ratcheting motion'' described by Gorman *et al.* [41] in cellular flames.

B. The rectangular system

1. Fluorinert FC70–47v10 silicone oil system

The flow regime diagram for this case, which appears in Fig. 16, indicates the temperature difference ΔT where stationary convection begins for various values of the lower layer depth fraction l_1. The temperature difference where time-dependent behavior begins is also indicated in Fig. 16. We find time dependence near onset in the range $0.365 \leqslant l_1 \leqslant 0.39$. Investigation down to a depth fraction $l_1 = 0.33$

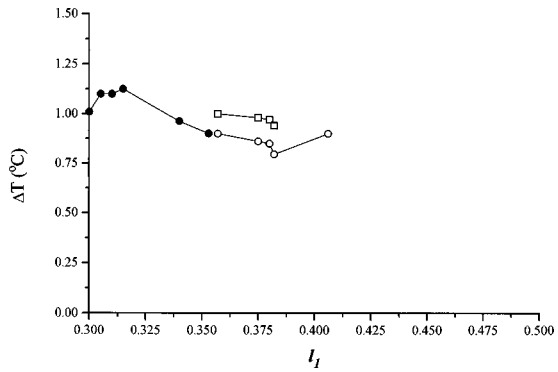

FIG. 12. Onset temperature difference to stationary thermal coupling (●), stationary mechanical coupling (○), and time-dependent (□) convection in the annular system using FC70 and 47v10 as the working fluids. Solid line serves only as a guide to the eye.

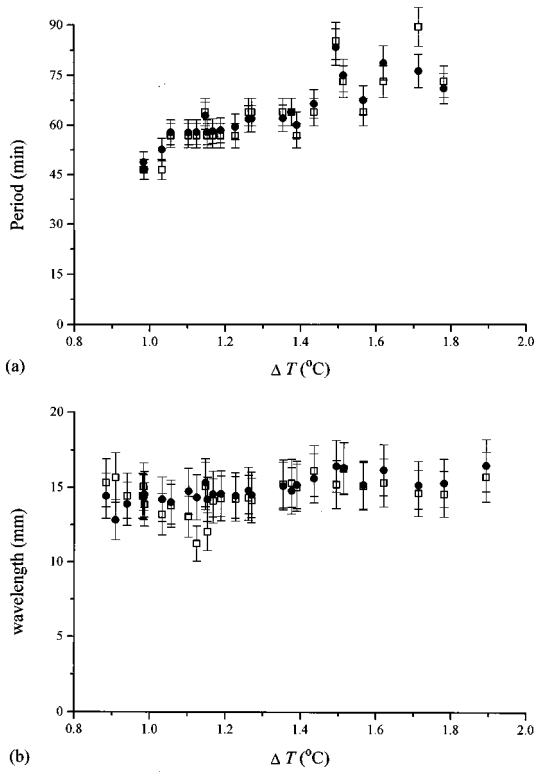

FIG. 13. (a) The period (τ) vs ΔT for $l_1 = 0.375$ from the annular system. (□) is lower layer, (●) is upper layer. (b) The wavelength (λ) vs ΔT. (□) is lower layer, (●) is upper layer.

shows that the system continues to exhibit thermal coupling at onset below the time-dependent region, growing stronger as ΔT is increased. As closer inspection of Fig. 16 shows, time dependence is only exhibited above the critical ΔT if the state at ΔT_c is mechanically coupled. A possible explanation for this phenomenon will be taken up below.

Observation of the system in the oscillatory state shows different behavior in each of the two layers. Typical behavior in the upper layer is a widening of a dark region near the center of the cell. Over time the large dark spot splits, a light region appearing between the two smaller dark regions, indicating the creation of a new roll. Correspondingly, a roll is annihilated near one end of the layer, keeping an approximately constant wavelength over time. The motion in the lower layer is typically a traveling wave, but the expansion and formation of new dark or light regions near the center of the cell is difficult to detect. The more vigorous action and motion of the upper layer causes the coupling to oscillate from mechanical to thermal away from the ends of the cell. To illustrate the variation in the coupling, we have plotted $|I_{\text{bottom}} - I_{\text{top}}|$, the absolute value of the intensity of the bottom layer minus the intensity of the top. Figure 17 shows the results of this treatment of the data. The dark regions show local thermal coupling between the two layers, while the light regions show mechanically coupled regions. We have observed two types of time-dependent motion with this combination of fluids. The first is the standing wave state shown in Fig. 17. The second is a traveling wave state where the rolls in both layers are moving, and the coupling is locked between the two layers as shown in Fig. 8. Both of these types of states are predicted to appear in the two-layer system [19], although traveling waves are only predicted in an infinite system. The appearance of either a traveling or stand-

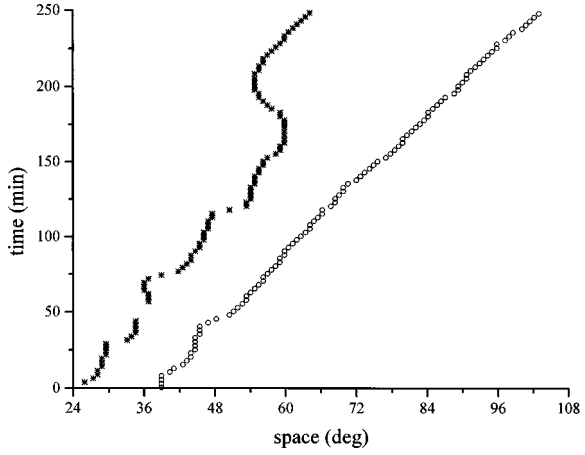

FIG. 14. One representative roll boundary taken from Fig. 10 (○) showing linear motion at $\Delta T = 1.189$ °C and Fig. 11 (∗) showing irregular motion at $\Delta T = 1.567$ °C, from the annular system. The roll at high ΔT is observed to change its direction of propagation.

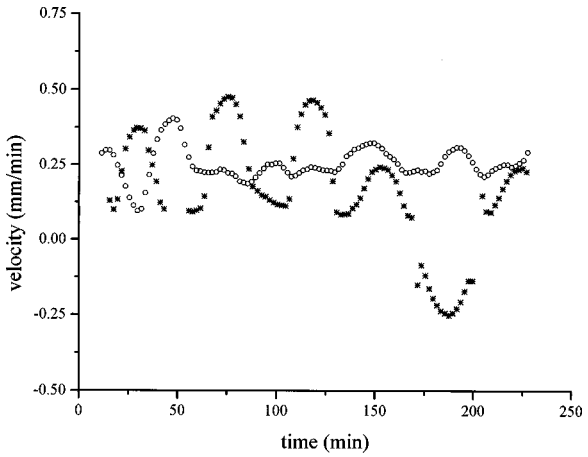

FIG. 15. Velocity vs time for the roll boundaries shown in Fig. 14. (○) at $\Delta T = 1.189$ °C, (∗) at $\Delta T = 1.567$ °C, from the annular system.

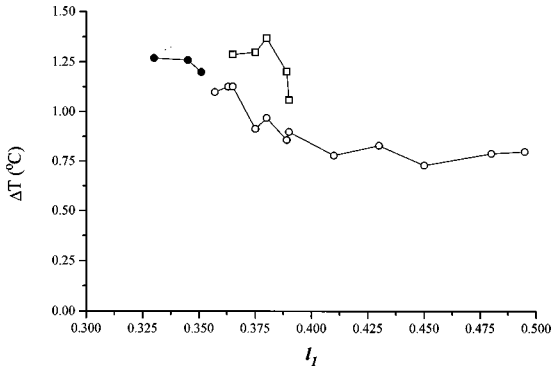

FIG. 16. Plot of ΔT vs depth fraction l_1 showing the range of coupling and the onset of oscillations. (○) indicates the onset of mechanically coupled stationary convection. (●) indicates the onset of thermally coupled stationary convection. (□) indicates the onset of time-dependent convection. Data from the rectangular system with FC70 and 47v10 as the working fluids.

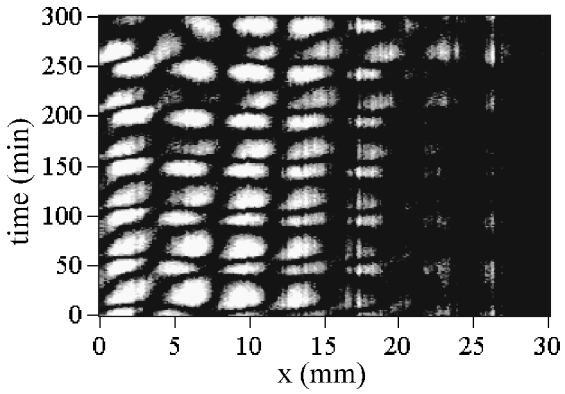

FIG. 17. Coupling variations demonstrated by $|I_{\text{bottom}}-I_{\text{top}}|$, for the standing wave state from the rectangular FC70-47v10 system. Dark regions show thermal coupling, light regions show mechanical coupling.

ing wave appears to be independent of ΔT, and shows a link to depth fraction, as shown in Table III.

We have calculated wave numbers and frequencies for the oscillations in both the top and bottom layers. The results are shown in Figs. 18 and 19, as a function of ΔT, for the depth fraction $l_1=0.39$. The constant values for varying ΔT imply that we are limited by the size of the cell, since at onset there are only 5–6 rolls in the cell.

2. Water–47v2 silicone oil system

The major difference between the FC70–47v10 fluid combination and the water-47v2 fluid combination lies in the much smaller value of $\gamma\beta r$ for the latter. This difference manifests itself in the appearance of time-dependent behavior at the onset of convection for a range of depth fractions $0.6\lesssim l_1\lesssim 0.71$, as illustrated in Fig. 20. Space-time plots of the behavior in the top layer are shown in Fig. 21 for the depth fraction $l_1=0.71$, with descriptions given in the captions. Only plots of the top layer are given because we could not achieve either shadowgraph or schlieren visualization in the water layer. We have used Kalliroscope particles and other tracers to confirm the existence of convection rolls in the lower layer, but they do not stay suspended long enough to allow study of the dynamics of the layer.

The measured periods and wave numbers for the top layer are shown in Fig. 22 at $l_1=0.71$ as a function of ΔT. The space-time plots (Fig. 21) show that the behavior of the system becomes more complex with increasing ΔT.

TABLE III. l_1 dependence of the coupling between layers in the rectangular FC70-47v10 system. SW denotes a standing wave and TW a traveling wave.

Depth fraction l_1	Coupling
0.390	SW
0.380	SW
0.371	SW
0.360	TW
0.357	TW

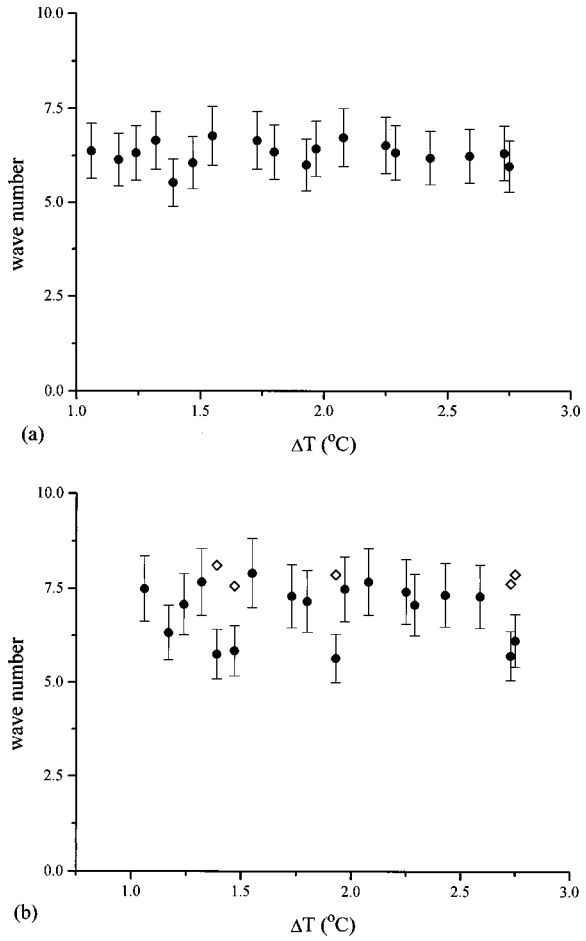

FIG. 18. Nondimensional wave numbers of the oscillations as a function of ΔT, for $l_1=0.39$ from the rectangular FC70-47v10 system. (a) Top layer; (b) lower layer; ($\diamond$) indicates the second of two wave numbers.

VI. DISCUSSION

A. Comparison of the two geometries

The primary physical difference between the annular and rectangular geometries is in the lateral end conditions on the roll structure. The rectangular system has end walls to restrict the motion of the rolls, while the annular system does not. A second difference is the size of the convection region. The rectangular cell typically has $\sim 5-6$ roll pairs while the annular cell has ~ 25 roll pairs.

These differences do not have an effect on the initial stationary convection in the case of FC70-47v10 as seen in Figs. 12 and 16. ΔT_c is nearly identical for the two systems, as is the type of coupling at onset. Additionally, the region of l_1 where time dependence is present is the same. Renardy [20] predicts a time-dependent region of $0.415\leqslant l_1\leqslant 0.417$, higher than observed here. The predicted onset $\Delta T=0.64\,^{\circ}\text{C}$ at $l_1=0.4$ is less than the experimental value of 0.9 °C. Likewise, the predicted ΔT for other l_1 are below the experimental values.

The differences in the geometries manifest themselves in the details of the patterns (summarized in Table IV). The first difference is in the wave number of the patterns. Renardy [20] predicts a range of $\alpha=4.5-5.5$ for the FC70-47v10 combination. The experiments find $\alpha\approx 7$ in the rectangular

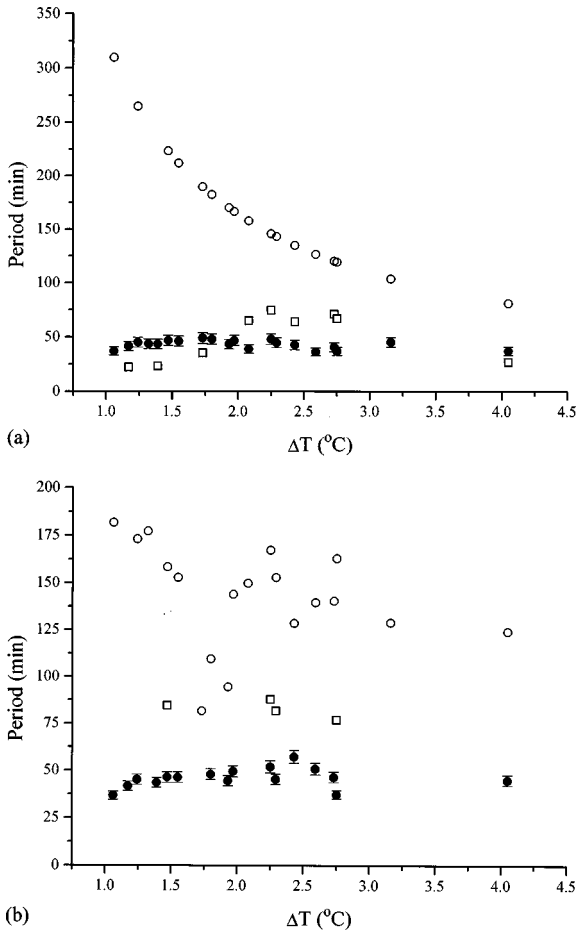

FIG. 19. Periods as a function of ΔT, for $l_1 = 0.39$ from the rectangular FC70-47v10 system. (●) indicates the primary oscillation period, (□) and (○) secondary and tertiary periods. (a) Top layer, (b) bottom layer.

system (Fig. 18) and $\alpha \approx 5.2$ in the annulus [Fig. 13(b)]. These measurements clearly show that the small size of the rectangular geometry is limiting the size of the rolls that are present in the flow.

A second difference is in ΔT at the onset to time dependence. Time dependence appears in the rectangular system at about 0.2 °C above the onset to convection while time dependence in the annular system is ≈0.1 °C above the stationary onset.

The periods of the time-dependent flow are nearly the same at onset. $\tau \approx 47$ min is found in the rectangle while $\tau \approx 50$ min in the annulus. Renardy [20] predicts $\tau \approx 40$ min. τ is essentially constant over the range of ΔT in the rectangular system (Fig. 19), while τ increases to ≈80 min at high ΔT in the annulus [Fig. 13(a)].

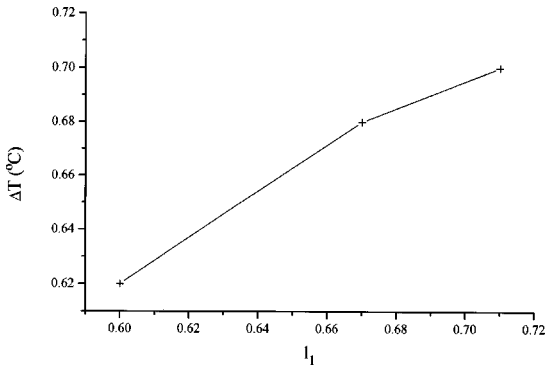

FIG. 20. Critical temperature difference ΔT_c for onset of convection for the rectangular water-47v2 system as a function of depth fraction l_1. The onset in all cases is oscillatory.

The last major differences between the convection in the two geometries concern the nature of the time-dependent flows. The annular geometry exhibits only traveling waves over the whole range in l_1, while the rectangular system exhibits both standing and traveling waves (Table III). This observation supports the predictions of Colinet and Legros [19] that only traveling waves should be observed in extended systems and standing waves in confined systems. Yet another variation is in the nature of the traveling waves. As discussed above, the traveling waves in the annular system show a stick-slip motion. The motion in the rectangular system is much smoother at an essentially constant velocity.

B. Comparison of the two fluid combinations

The appearance of time-dependent activity at or near onset has been found in other pattern forming physical systems, most notably the miscible two-fluid problem, i.e., double diffusive convection [6], and Taylor-Dean flow [42,43]. The trait that these systems share is a competition between instabilities. In double diffusive convection, the competition is between a destabilizing buoyancy force and a stabilizing concentration gradient. Colinet and Legros [19] note that the form of their equations for traveling waves in the two-layer system is identical to those obtained by Knobloch [44] for traveling waves in binary fluid convection. The Taylor-Dean system exhibits a competition between a centrifugal instability (Taylor-Couette flow), and the instability caused by pressure driven flow in a curved channel (Dean flow). In the immiscible two-layer Rayleigh-Bénard system, the competition is between the stabilizing effect of surface tension at the interface between the two fluids, and the heat transport at the interface. A possible mechanism for the variation in coupling is the following, originally postulated by Gershuni and Zhukovitskii [7]. The onset of convection in the lower (or

TABLE IV. Comparison between experiments in annular and rectangular geometries and theory for the FC70-4v10 fluid combination.

	Annulus	Rectangular	Theory [20]
Wave number	5.2	7	4.5–5.5
Period at onset (min)	47	50	40
Period at high ΔT (min)	80	50	
l_1 with time dependence	0.357–0.382	0.365–0.390	0.415–0.417

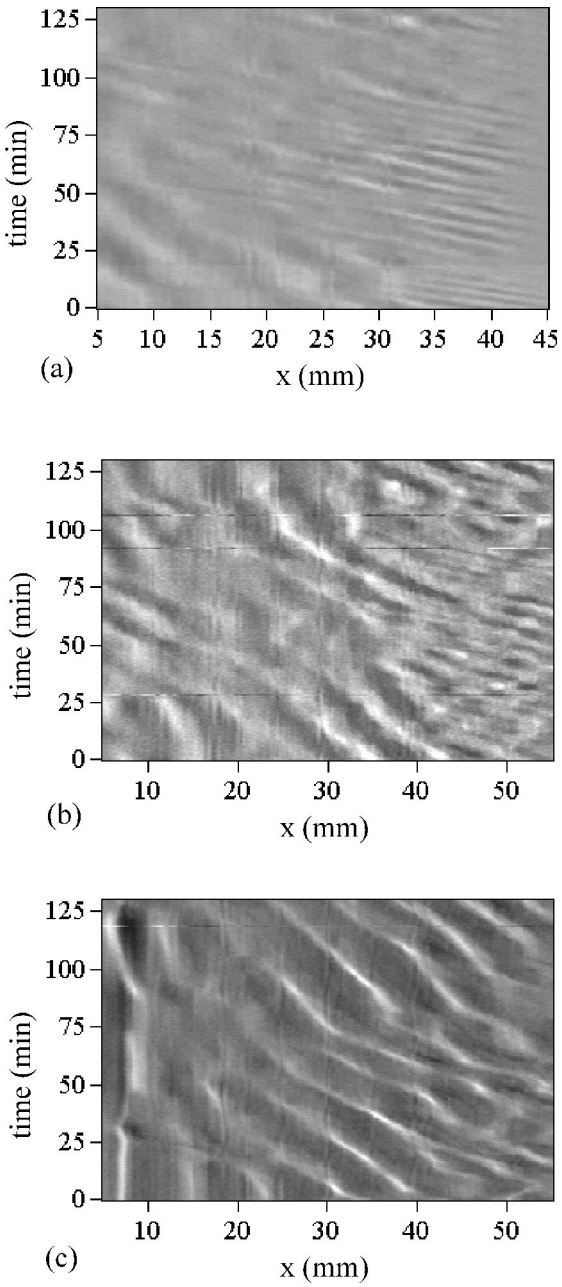

FIG. 21. Background-subtracted space-time plots of the top layer in the rectangular 47v2-water system for (a) $l_1=0.71$, $\Delta T=1.01\,^{\circ}\mathrm{C}$, (b) $l_1=0.71$, $\Delta T=1.14\,^{\circ}\mathrm{C}$, and (c) $l_1=0.71$, $\Delta T=1.5\,^{\circ}\mathrm{C}$.

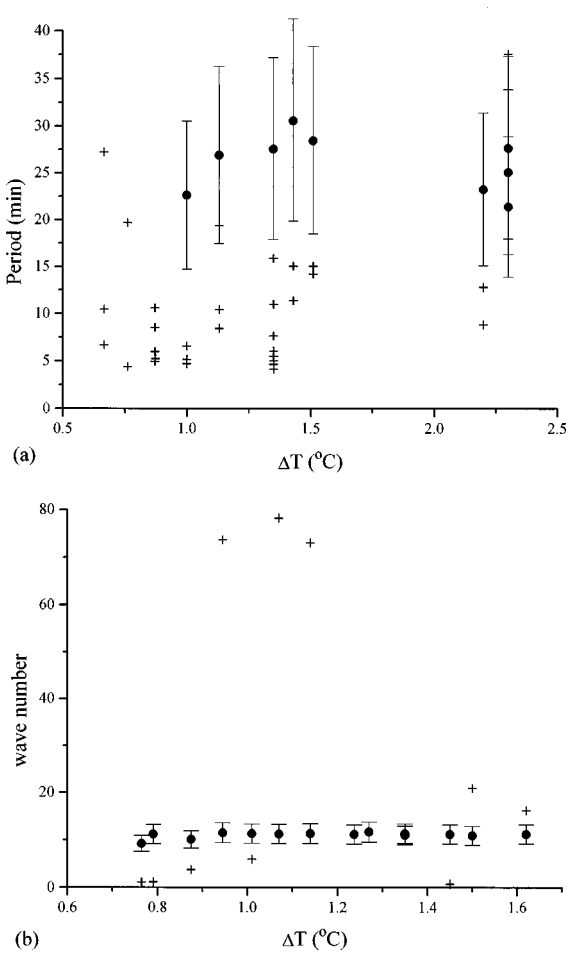

FIG. 22. Top layer pattern characteristics as a function of ΔT for $l_1=0.71$ from the rectangular water-47v2 system. (a) Periods, (●) indicates the primary oscillation period; (+) secondary periods. (b) Wave numbers, (●) indicates the primary wave number, (+) indicate secondary wave numbers.

upper) layer will induce the upper (lower) layer into mechanical coupling through the continuity of tangential velocity at the interface. If sufficient heat is transported to the interface by the lower fluid, a hot spot may form at the bottom of the upper layer. Enough thermal energy at this point may cause the fluid to rise, thereby reversing the direction of circulation in the upper layer. The surface tension then plays the role of the restoring force, reverting the circulation to a mechanically coupled state when enough energy is removed from the hot spot. It is apparent that for thin lower layers, the amount of heat lost in an upwelling stream due to thermal diffusion or viscous dissipation is small, and the amount of thermal energy transported to the interface is always large enough to induce upwellings directly above the rising streams in the lower fluid, leading to a time-independent state of thermal coupling. On the other hand, if the lower layer is thick, then there is never enough thermal energy transported to the interface to induce thermal coupling, and the coupling remains mechanical and time independent. The interesting behavior occurs at intermediate depth fractions, where the energy balance is delicate enough to allow oscillations to appear. The significance of $\gamma\beta r$ is also more apparent from this scenario, as it compares the conductivity, expansivity, and density of the two fluids. For example, $\gamma\beta r \gg 1$ implies that these quantities are larger in the lower fluid. Moreover, if the heat transport is higher in the lower fluid, it would be easier to create a situation where oscillations could occur. In our case, where $\gamma\beta r$ is smaller than 1, a cold spot could form at the top of the lower layer, which could induce a flow reversal in that layer and hence oscillations.

VII. CONCLUSION

We have explored the quasi-two-dimensional two-layer Rayleigh-Bénard system with two distinct geometries, rectangular and annular, using Fluorinert™ FC70 and 47v10 silicone oil as the working fluids. We have also used water and 47v2 silicone oil in the rectangular system. We used optical

methods to probe the flow in both geometries.

The FC70-47v10 fluid combination exhibits time-dependent states slightly above the onset to stationary convection in both geometries. The wave number is constant throughout the range of ΔT with $\alpha \approx 5.2$ for the annular system, inside the predicted range. The rectangular system shows $\alpha \approx 7$, slightly above the predicted range. The onset periods are similar in both systems, being about 50 min, slightly above the predicted 40 min. The period is constant in the rectangular system, while it increases to about 80 min in the annular system as ΔT is increased. The time-dependent states in the annular system take the form of traveling waves for the range of l_1. Both traveling and standing waves are observed in the rectangular system. Finally, the traveling waves in the annular system exhibit stick-slip motion while the motion in the rectangular system is smoother.

Since the FC70-47v10 combination does not show time dependence coincident with the onset to convection, Renardy's parameter ($\gamma\beta r$) [20] has been used during the search for a second set of fluids. $\gamma\beta r = 0.776$ for the FC70-47v10 combination is too near one to exhibit time dependence at onset. However, the combination of water and 47v2 with $\gamma\beta r = 0.375$ does show time dependence coincident with the onset to convection, thus confirming the role of $\gamma\beta r$ in predicting the likelihood of observing a time-dependent onset state.

ACKNOWLEDGMENTS

The authors are grateful to Y. Renardy, P. Kolodner, and S. Morris for fruitful discussions. This project was supported by NASA Microgravity Grant No. NAG3-1612.

[1] M. C. Cross and P. C. Hohenberg, Rev. Mod. Phys. **65**, 851 (1993).
[2] C. D. Andereck, S. S. Liu, and H. L. Swinney, J. Fluid Mech. **164**, 155 (1986).
[3] T. E. Faber, *Fluid Dynamics for Physicists* (Cambridge University Press, Cambridge, England, 1995).
[4] I. Mutabazi, J. J. Hegseth, C. D. Andereck, and J. E. Wesfreid, Phys. Rev. Lett. **64**, 1729 (1990).
[5] M. M. Degen, W. J. Kahle, and C. D. Andereck, Phys. Rev. E **57**, 1761 (1998).
[6] P. Kolodner, D. Bensimon, and C. M. Surko, Phys. Rev. Lett. **60**, 1723 (1988).
[7] G. Z. Gershuni and E. M. Zhukovitskii, Dokl. Akad. Nauk SSSR **265**, 302 (1982) [Sov. Phys. Dokl. **27**, 531 (1982)].
[8] C. Normand, Y. Pomeau, and M. G. Velarde, Rev. Mod. Phys. **49**, 581 (1977).
[9] L. Rayleigh, Philos. Mag. **32**, 528 (1916).
[10] F. Daviaud, M. Dubois, and P. Bergé, Europhys. Lett. **9**, 441 (1989).
[11] Y. Renardy and D. D. Joseph, *Fundamentals of Two Fluid Dynamics*, Interdisciplinary Applied Mathematics Vol. 1 (Springer-Verlag, Reading, MA, 1993).
[12] F. M. Richter and C. E. Johnson, J. Geophys. Res. **79**, 1635 (1974).
[13] F. M. Richter and D. P. McKenzie, J. Geophys. Res. **86**, 6133 (1981).
[14] L. Cserepes and M. Rabinowicz, Earth Planet. Sci. Lett. **76**, 193 (1985).
[15] L. Cserepes, M. Rabinowicz, and C. Rosemberg-Borot, J. Geophys. Res. **93**, 12 009 (1988).
[16] F. H. Busse, Phys. Earth Planet. Inter. **24**, 320 (1981).
[17] A. Prakash and J. N. Koster, Microgravity Q. **4**, 46 (1994).
[18] M. Renardy and Y. Renardy, Physica D **32**, 227 (1988).
[19] P. Colinet and J. C. Legros, Phys. Fluids **6**, 2631 (1994).
[20] Y. Renardy, Z. Angew. Math. Phys. **47**, 567 (1996).
[21] S. Rasenat, F. H. Busse, and I. Rehberg, J. Fluid Mech. **199**, 519 (1989).
[22] Y. Renardy (private communication).
[23] Y. Renardy and D. D. Joseph, Phys. Fluids **28**, 788 (1985).
[24] Y. Renardy, Phys. Fluids **29**, 788 (1986).
[25] Y. Renardy and M. Renardy, Phys. Fluids **28**, 2699 (1985).
[26] K. Fujimura and Y. Renardy, Physica D **85**, 25 (1995).
[27] R. W. Zeren and W. C. Reynolds, J. Fluid Mech. **53**, 305 (1972).
[28] M. R. E. Proctor and C. A. Jones, J. Fluid Mech. **188**, 301 (1988).
[29] A. Prakash and J. N. Koster, Trans. ASME, J. Heat Transfer **118**, 366 (1996).
[30] H. C. Nataf, S. Moreno, and P. Cardin, J. Phys. (France) **49**, 1707 (1988).
[31] P. Cardin and H. C. Nataf, Europhys. Lett. **14**, 665 (1991).
[32] P. Cardin, H. C. Nataf, and P. Dewost, J. Phys. II **1**, 599 (1991).
[33] C. D. Andereck, P. W. Colovas, and M. M. Degen, in *Advances in Multi-Fluid Flows*, edited by Y. Y. Renardy, A. V. Coward, D. T. Papageorgiou, and S.-M. Sun (AMS-IMS-SIAM, Philadelphia, 1996), pp. 3–12.
[34] C. D. Andereck, P. W. Colovas, and M. M. Degen, in *Proceedings of the Third Microgravity Fluid Physics Conference*, NASA Conf. Publ. No. 3338 (NASA, Cleveland, OH, 1996).
[35] P. W. Colovas, Ph.D. dissertation, The Ohio State University, 1996.
[36] F. H. Busse and G. Sommerman, in *Advances in Multi-Fluid Flows*, edited by Y. Y. Renardy, A. V. Coward, D. T. Papageorgiou, and S.-M. Sun (AMS-IMS-SIAM, Philadelphia, 1996), pp. 33–41.
[37] R. J. Goldstein, *Fluid Mechanics Measurements* (Springer-Verlag, Berlin, 1983).
[38] D. R. Jenkins, J. Fluid Mech. **190**, 451 (1988).
[39] P. Bergé, Phys. Scr. **40**, 381 (1989).
[40] M. F. Schatz *et al.*, in *Proceedings of the Second Microgravity Fluid Physics Conference*, NASA Conf. Publ. No. 3276 (NASA, Cleveland, OH, 1994).
[41] M. Gorman, M. el Hamdi, B. Pearson, and K. A. Robbins, Phys. Rev. Lett. **76**, 228 (1996).
[42] I. Mutabazi, J. J. Hegseth, and C. D. Andereck, Phys. Rev. A **38**, 4752 (1988).
[43] I. Mutabazi, J. J. Hegseth, and C. D. Andereck, Phys. Rev. Lett. **64**, 1729 (1990).
[44] E. Knobloch, Phys. Rev. A **34**, 1538 (1986).